Dynamics of bacteriorhodopsin 2D crystal observed by high-speed atomic force microscopy.

Dynamics of bacteriorhodopsin 2D crystal observed by high-speed atomic force microscopy

Hayato Yamashita [a,*], Kislon Voïtchovsky [b], Takayuki Uchihashi [a,c], Sonia Antoranz Contera [b], John F. Ryan [b], Toshio Ando [a,c]

[a] Department of Physics, Kanazawa University, Kakuma-machi, Kanazawa, Japan
[b] Physics Department, University of Oxford, Parks Road, OX1 3PU, Oxford, UK
[c] CREST/JST, Sanban-cho, Chiyoda-ku, Tokyo, Japan.

(Received)

*Corresponding author. Tel: +81-762-64-5928. Fax: +81-762-64-5739.
E-mail: yhayato@stu.kanazawa-u.ac.jp

A B S T R A C T

We have used high-speed atomic force microscopy to study the dynamics of bacteriorhodopsin (bR) molecules at the free interface of the crystalline phase that occurs naturally in purple membrane. Our results reveal temporal fluctuations at the crystal edges arising from the association and dissociation of bR molecules, most predominantly pre-formed trimers. Analysis of the dissociation kinetics yields an estimate of the inter-trimer single-bond energy of –0.9 kcal/mol. Rotational motion of individual bound trimers indicates that the inter-trimer bond involves W10-W12 tryptophan residues.

Keywords:

High-speed atomic force microscopy; bacteriorhodopsin; Two-dimensional crystal; Dynamic equilibrium; Trimer; Molecular interaction

1. Introduction

The current view of cell membrane structure derives from the fluid mosaic model in which proteins are considered to diffuse freely within a fluid lipid bilayer (Singer and Nicolson, 1972). The first direct evidence for protein diffusion within cell membranes was provided by hybrid cell experiments (Frye and Edidin, 1970). Since then, various techniques including fluorescence recovery after photobleaching microscopy (Swaminathan et al., 1997) and single particle tracking microscopy (Kusumi et al., 1993) have provided a more detailed understanding of the mobile nature of proteins in biological membranes. In particular, it has been shown that proteins in native membranes may not diffuse freely but are in fact confined to specific domains. Cells use several confining mechanisms such as anchoring to the cytoskeleton through hetero-bifunctional proteins (Byers and Branton, 1985), diffusion barriers formed by the accumulation of proteins anchored to cytoskeleton meshes (Halenda et al., 1987; Nakada et al., 2003), or self-assembly into large two-dimensional (2D) crystalline patches, as in the case of bacteriorhodopsin (bR), a light-driven proton pump found in the so-called purple membranes (PM) of Halobacterium salinarum (Blaurock, 1971). Despite these advances, an understanding of the membrane dynamics at the nanoscale remains a major challenge due primarily to the lack of measurement techniques allowing simultaneous spatial and temporal observation of single molecules within native membranes.

In this paper, we introduce a new technique for observing membrane protein dynamics, high-speed atomic force microscopy (HS-AFM) (Ando et al., 2001; Ando et al., 2008), which provides both high spatial (~1 nm) and temporal (40 ms/image) resolution of single molecules in their native environment. We have used this technique to study the dynamics of bR crystal formation at the edges of native PM. PM is composed of bR trimers which are arranged in a hexagonal lattice (Henderson et al., 1990). We directly imaged the dynamic events occurring at the interface between crystalline and disordered areas of PM. Fitting our results with a simple model,

we were able to estimate the energy of the trimer-trimer interaction and the degree of oligomerization of bR in the non-crystal region. Our results also highlight the role played by certain residues of bR (W10-12) in the interactions between trimers.

2. Materials and methods

2.1. Sample preparation

PM from the NRL strain of Halobacterium salinarum was isolated following standard procedures (Oesterhelt and Stoeckenius, 1974). The purest fraction obtained by sucrose density gradient centrifugation was frozen and stored at 193 K. After thawing and then removing sucrose by sedimentation, the pellet was suspended in a solution (Buffer-A) containing 10 mM Tris-HCl (pH 8.0) and 300 mM KCl. The sample (1.7 mg/ml) was kept at 277 K before AFM experiments. For AFM observation, the sample was diluted to ~0.1 mg/ml in Buffer-A.

2.2. HS-AFM observation

The laboratory-built tapping mode HS-AFM apparatus used here is an extensively improved version of the AFM previously reported (Ando et al., 2001). The cantilever deflection sensor was specially optimized for bR observations and equipped with a 980 nm infrared laser. The laser beam was focused onto a small cantilever using a ×50 objective lens (Olympus). The cantilever (Olympus) has a resonant frequency of ~1 MHz in water and a spring constant of 0.1-0.2 N/m. An amorphous carbon tip was grown on the original cantilever tip by electron beam deposition. The tip length was adjusted to about 1 μm and the tip apex was sharpened by plasma etching (~4 nm in radius) (Ando et al., 2008). A sample stage made of quartz glass was placed on the z-scanner and a 1.5 mm diameter mica disk was glued onto the sample stage. A 2 μl sample droplet was then deposited on the freshly cleaved mica surface and incubated for 3 min. All HS-AFM measurements were performed under solution (Buffer-A) at room temperature. Both the membrane and the atomically flat mica substrate possess a strong hydration shell which prevents direct binding of PM to the mica, and the adsorption occurs through non-specific electrostatic forces. A water-layer of thickness ~1 nm separates the membrane from the mica surface allowing motion of membrane proteins within the membrane (Kim et al., 2001; Sackmann, 1996).

Control experiments with simple supported lipid bilayers ensured that the effective experimental temperature of the sample was lower than 310 K, judging from the gel phase transition of the lipids (not shown). To estimate the inter-trimer association energy in the photo-activated state, a green laser (532 nm, 20 μW) was directed through the objective lens onto the sample. This low-power irradiation is sufficient for exciting all bR molecules in the observed area but does not damage the sample.

3. Results and Discussion

3.1. High-resolution images of 2D crystal of bacteriorhodopsin in PM

PM exhibits flat, round-shape patches typically 1-5 μm in diameter. In the patch shown in Fig. 1A, a 2D crystal lattice of bR is formed over the inner region (surrounded by the dotted line), whereas in the peripheral outer region, there is no crystalline order. Figure 1B shows a high magnification image of the inner region of the cytoplasmic leaflet captured at 1 frame/sec. The distinction of PM cytoplasmic and extracellular sides was made using the high-resolution AFM image as previously reported (Müller et al., 1996; Voitchovsky et al., 2006). The hexagonal lattice of bR trimers is clearly visible, demonstrating the ability of our HS-AFM apparatus to visualize individual bR molecules even at high imaging rate. Two higher magnification images of an edge region of PM acquired successively at 1 frame/sec (with an interframe time of a few ms) are presented in Fig. 1C and d, respectively. They both exhibit a distinct border between the crystal and non-crystalline area. The shape of the border differs between the two images (arrows), indicating that the crystal is in dynamic equilibrium with bR molecules located in the non-crystalline area. In fact, “noise” spikes were frequently observed in the non-crystalline area, most likely produced by diffusing bR molecules moving too fast to be clearly resolved at 1 frame/sec.

3.2. Association and dissociation of bR molecules at crystal edges

To investigate the details of the dynamic structural changes occurring at the crystal edge, a time sequence of higher magnification images of the boundary region was acquired (see Fig. 2 and Supplementary movie 1). The darker regions in the images correspond to non-crystalline areas. The bR trimers in the crystal are indicated by the thinlined triangles. At 0.6 sec (Fig. 2A), two bR trimers (red triangles) have newly bound to the crystal edge. At 2.1 sec (Fig. 2A), two bR trimers (white triangles) have dissociated and another trimer (red triangle) has bound to the crystal edge. One of the two dissociated trimers remained in the crystal area for ~0.9 sec. Not only bR trimers but also bR dimers and monomers were observed to bind to and dissociate from the crystal edge. A bR dimer (red rectangle in Fig. 2B) stayed bound to the edge for ~0.5 sec, whereas a bR monomer (red circle in Fig. 2C) remained bound to the edge for ~0.4 sec. These residence times for monomers and dimers are shorter than those of the trimers. Table 1 summarizes 239 observed binding events, classified according to their oligomerization states. The binding of trimeric bR occurred predominantly (82 %), whereas binding of dimeric bR (6.7 %) was only about half that of monomeric bR (11.3 %).

3.3. Pivotal motion of weakly bound bR trimer

On rare occasions, we observed large crevasses in the crystal as exemplified in Fig. 3A (area surrounded by the dotted line). In the crevasse, the two-dimensional lattice structure is not present, and consequently bR trimers are loosely packed and exhibit appreciable motion, which is restricted to some extent by the interaction with the surrounding bR molecules. At the interface between the

dense crystal area and the non-crystalline area, pivotal motion of bR trimers was often observed. As shown by the AFM images taken at 25 frames/sec (Fig. 3B), the bR trimer (red triangle) rotated counterclockwise around the inter-trimer bond (arrow, compare the images at 0 sec and 0.24 sec) and subsequently oscillated around the same position for more than 2 sec. At 2.88 sec, the trimer rotated back to its initial position (see Supporting Movie 2). This pivotal motion was repeatedly observed. Although we noted similar motion at the distinct interface between the crystalline and non-crystalline areas like the one shown in Fig. 2, the pivotal motion was too fast to be clearly imaged.

We interpret this pivotal motion as a direct effect of the inter-trimer bonds. Static images of PM with molecular or submolecular resolution reveal the parts of a bR molecule which lie in close proximity with the neighboring trimers (Fig. 1B). However, such images do not necessarily show the actual location of the inter-trimer bonds since such proximity may occur passively and non-specifically. On the other hand, HS-AFM movies can localize the main inter-trimer bond from the trimer pivot point. Neutron diffraction studies and structural comparison with halorhodopsin (hR) indicate that a tryptophan residue (W12) participates in lattice formation (Oesterhelt, 1995; Weik et al., 1998). In addition, it has been shown that the double mutation (W12I/W80I) leads to collapse of the 2D bR crystal and monomerization of bR trimers (Sapra et al., 2006). Furthermore, force spectroscopy experiments have highlighted the role of W10-12 in anchoring bR into the PM lattice through steric-specific interactions (Voitchovsky et al., 2007). Fig. 3C shows a schematic reconstruction of Fig. 3B using the pdb structure of bR trimers (L.O. Essen, 1998) with the positions of W12 highlighted (white spheres). When comparing the AFM images with the corresponding model, the trimer appears to pop out of the crystal due to breaking of bonds localized near W12 residues (indicated by the arrows in Fig. 3C), subsequently it rotates through another W12 residue (circled by the dotted line) and is finally re-trapped at the crystal edge.

3.4. Quantitative analysis of intertrimer interaction energy

In order to estimate the inter-trimer interaction energy, we analyzed the residence time of newly bound bR trimers at the crystal edge and its dependence on the number of interaction sites. In addition, we examined the effect of bR photo-activation on the residence time since the protein photo-isomerization can, in principle, affect the membrane dynamics at larger scale (Manneville et al., 1999). For our analysis, we assumed that within the two-dimensional bR crystal, a trimer can interact with the surrounding trimers through six sites, each based on a W12 residue as indicated by the dotted lines in 'VI' of Fig. 4A. Following the same model, the number of interaction sites at the crystal edge is reduced, depending on the binding position, as indicated by 'I', 'II', and 'III' in Fig. 4A. Successive AFM images as exemplified in Fig. 2 showed many binding and dissociation events in which bR trimers bound to different sites at the border between the crystal and non-crystal areas. These events can be classified into types 'I', 'II', and 'III' depending on the number of interaction sites involved. Type II binding events are predominant (~74%), whereas type I (~6 %) and type III

(~20%) events are less frequent. The lifetime of the type I bonds was too short to obtain clear images of the corresponding event, preventing reliable statistics.

Fig. 4B shows a histogram of the lifetime of type II bonds which was measured using AFM images taken at 10 frames/s (tip velocity, 75 μm/s). This histogram could be well fitted by a single exponential (correlation coefficient, $r = 0.9$), from which the average lifetime τ_2 was estimated to be 0.19±0.01 sec. To ensure that the observed dissociation events are not significantly affected by the AFM tip during the scanning, we examined the dependence of the average lifetime on the tip velocity when a constant scanning force is maintained. The inset in Fig. 4B shows the average lifetime as a function of the tip velocity and indicates that the average lifetime is about 0.17±0.06 sec, irrespective of the tip velocity. Thus, we conclude that the tip-sample interaction does not significantly affect the natural association and dissociation kinetics of the bR trimer. Fig. 4C shows a histogram of the type III bond lifetime, from which the average lifetime τ_3 was estimated to be 0.85±0.08 sec. The longer lifetime of type III bonds compared with type II obviously arises from a relationship of $E_3 < E_2 < 0$, where E_2 and E_3 are the association energies responsible for type II and type III interactions, respectively (Yamamoto et al., 2008). The average lifetime ratio, τ_2/τ_3, is given by

$$\tau_2/\tau_3 = exp[(E_3 - E_2)/k_B T], \qquad (1)$$

where k_B is Boltzmann's constant and T is the temperature in Kelvin. Because the type II interaction contains two elementary bonds, whereas the type III interaction contains three (see Fig. 4A), the energy difference $E_3 - E_2$ corresponds to the association energy of the single elementary bond. From the ratio $\tau_2/\tau_3 = 0.22$ and Eq. (1), this elementary association energy is estimated to be about $-1.5\ k_B T$, which corresponds to –0.9 kcal/mol at 300 K.

A previous study of differential scanning calorimetry on the 2D bR crystal showed two calorimetric transitions (Jackson and Sturtevant, 1978): a reversible transition at 70~80 °C and an irreversible transition at ~100 °C. The reversible transition was interpreted as melting of the lattice structure, which was later confirmed by X-ray diffraction studies of hydrated PM (Koltover, 1999). A low degree of order is indeed retained at temperatures slightly above the melting temperature, which likely corresponds to bR trimers. The energy required for melting the lattice structure is estimated to be 6~7 kcal/mol (Jackson and Sturtevant, 1978). This value approximately coincides with -6×0.9 kcal/mol estimated by our AFM study for the association energy in the full interaction of a trimer with the surrounding lattice (type VI).

In order to assess the possible effect of photo-induced structural changes of bR on the PM lattice dynamics, we measured τ_2 and τ_3 for illuminated PM. However, we did not observe any appreciable difference with the corresponding lifetimes measured for dark adapted membrane. Our observation contrasts with the results of Kahya et al. who reported a decreased lateral mobility for photo-activated bR molecules due to formation of clusters comprising two or three trimers (Kahya et al., 2002). Their results, however, relied on fluorescence correlation spectroscopy and freeze-fracture electron microscopy of bR reconstituted in model membranes (giant unilamellar

vesicles). We believe this discrepancy can be explained by differences in the constituent lipids of the native and model membranes. PM native lipids are indeed known to be essential for bR crystallization (Sternberg et al., 1993) and dynamics (Hendler and Bose, 2003).

4. Conclusion

We have succeeded in measuring association-dissociation dynamics of bR at the edges of a native PM crystal at the single molecule level using HS-AFM. The results provide a direct observation of the mechanisms of PM lattice co-translational assembly and strongly support the hypothesis that bR trimers are preformed before being assembled into the crystal (Krebs and Isenbarger, 2000). Our AFM movies also highlight the presence of a pivot point for the rotational motion of bR trimers bound to the PM edge region, demonstrating the presence of a specific inter-trimer bond near the W12 residue. Consistently, the average residence times of bR trimers bound to the crystal edge depended on the number of bonds formed, allowing us to estimate the association energy of the single bond to be –0.9 kcal/mol, in good agreement with differential scanning calorimetry measurements. Thus, our approach provides a good estimate of the inter-trimer association energy. As demonstrated here with PM, the unique ability of HS-AFM to provide simultaneous high spatial and temporal resolution opens new avenues for studying the dynamics of native biological systems.

Acknowledgments

We acknowledge Dr. Daisuke Yamamoto for valuable discussions. This work was supported by the JST CREST project, the JST project of Development of Systems and Technology for Advanced Measurement and Analysis, and the Strategic International Cooperative Program of the JST with a Grant-in-Aid for Scientific Research on Priority Areas, a Grant-in-Aid for Basic Research (S) from the MEXT Japan, and a Grant-in-Aid for JSPS Fellows (to HY). This work was also supported by the Bionantechnology IRC and a BBSRC JPA. KV acknowledges funding from the Lord Florey fellowship.

Reference

Ando, T., Kodera, N., Takai, E., Maruyama, D., Saito, K., Toda, A. 2001. A high-speed atomic force microscope for studying biological macromolecules. Proc. Natl. Acad. Sci. USA 98, 12468-12472.

Ando, T., Uchihashi, T., Kodera, N., Yamamoto, D., Miyagi, A., Taniguchi, M., Yamashita, H. 2008. High-speed AFM and nano-visualization of biomolecular processes. Pflugers Arch. 456, 211-225.

Blaurock, A. E., Stoeckenius, W,. 1971. Structure of the purple membrane. Nature New Biol. 233, 152-154.

Byers, T. J., Branton, D. 1985. Visualization of the protein associations in the erythrocyte membrane skeleton. Proc. Natl. Acad. Sci. USA 82, 6153-6157.

Frye, L. D., Edidin, M. 1970. The rapid intermixing of cell surface antigens after formation of mouse-human heterokaryons. J. Cell Sci. 7, 319-335.

Halenda, R. M., Primakoff, P., Myles, D. G. 1987. Actin filaments, localized to the region of the developing acrosome during early stages, are lost during later stages of guinea pig spermiogenesis. Biol. Reprod. 36, 491-499.

Henderson, R., Baldwin, J. M., Ceska, T. A., Zemlin, F., Beckmann, E., Downing, K. H. 1990. Model for the structure of bacteriorhodopsin based on high-resolution electron cryo-microscopy. J. Mol. Biol. 213, 899-929.

Hendler, R. W., Bose, S. 2003. Interconversions among four M-intermediates in the bacteriorhodopsin photocycle. Eur. J. Biochem. 270, 3518-3524.

Jackson, M. B., Sturtevant, J. M. 1978. Phase transitions of the purple membranes of Halobacterium halobium. Biochemistry 17, 911-915.

Kahya, N., Wiersma, D. A., Poolman, B., Hoekstra, D. 2002. Spatial organization of bacteriorhodopsin in model membranes. Light-induced mobility changes. J. Biol. Chem. 277, 39304-39311.

Kim, J., Kim, G., Cremer, P. S. 2001. Investigations of water structure at the solid/liquid interface in the presence of supported lipid bilayers by vibrational sum frequency spectroscopy. Langmuir 17, 7255-7260.

Koltover, I., Raedler, J.O., Salditt, T., Rothschild, K.J., Safinya, C.R. 1999. Phase behavior and interactions of the membrane-protein bacteriorhodopsin. Phys. Rev. Lett. 82, 3184-3187.

Krebs, M. P., Isenbarger, T. A. 2000. Structural determinants of purple membrane assembly. Biochim. Biophys. Acta 1460, 15-26.

Kusumi, A., Sako, Y., Yamamoto, M. 1993. Confined lateral diffusion of membrane receptors as studied by single particle tracking (nanovid microscopy). Effects of calcium-induced differentiation in cultured epithelial cells. Biophys. J. 65, 2021-2040.

L.O. Essen, R. S., W.D. Lehmannn, D. Oesterhelt. 1998. Lipid patches in membrane protein oligomers: Crystal structure of the bacteriorhodopsin-lipid complex. Proc. Natl. Acad. Sci. USA 95, 11673-11678.

Manneville, J.-B., Bassereau, P., Levy, D., Prost, J. 1999. Activity of Transmembrane Proteins Induces Magnification of Shape Fluctuations of Lipid Membranes. Phys. Rev. Lett. 82, 4356-4359.

Müller, D. J., Schoenenberger, C. A., Buldt, G., Engel, A. 1996. Immuno-atomic force microscopy of purple membrane. Biophys. J. 70, 1796-1802.

Nakada, C., Ritchie, K., Oba, Y., Nakamura, M., Hotta, Y., Iino, R., Kasai, R. S., Yamaguchi, K., Fujiwara, T., Kusumi, A. 2003. Accumulation of anchored proteins forms membrane diffusion barriers during neuronal polarization. Nature Cell Biol. 5, 626-632.

Oesterhelt, D. 1995. Structure and function of halorhodopsin. Israel J. Chem. 35, 475-494.

Oesterhelt, D., Stoeckenius, W. 1974. Isolation of the cell membrane of Halobacterium halobium and its fractionation into red and purple membrane. Methods Enzymol. 31, 667-678.

Sackmann, E. 1996. Supported membranes: scientific and practical applications. Science 271, 43-48.

Sapra, K. T., Besir, H., Oesterhelt, D., Muller, D. J. 2006. Characterizing molecular interactions in different bacteriorhodopsin assemblies by single-molecule force spectroscopy. J. Mol. Biol. 355, 640-650.

Singer, S. J., Nicolson, G. L. 1972. The fluid mosaic model of the structure of cell membranes. Science 175, 720-731.

Sternberg, B., Watts, A., Cejka, Z. 1993. Lipid-induced modulation of the protein packing in two-dimensional crystals of bacteriorhodopsin. J. Struct. Biol. 110, 196-204.

Swaminathan, R., Hoang, C. P., Verkman, A. S. 1997. Photobleaching recovery and anisotropy decay of green fluorescent protein GFP-S65T in solution and cells: cytoplasmic viscosity probed by green fluorescent protein translational and rotational diffusion. Biophys. J. 72, 1900-1907.

Voitchovsky, K., Contera, S. A., Kamihira, M., Watts, A., Ryan, J. F. 2006. Differential Stiffness and Lipid Mobility in the Leaflets of Purple Membranes. Biophys. J. 90, 2075-2085.

Voitchovsky, K., Contera, S. A., Ryan, J. F. 2007. Electrostatic and steric interactions determine bacteriorhodopsin single-molecule biomechanics. Biophys. J. 93, 2024-2037.

Weik, M., Patzelt, H., Zaccai, G., Oesterhelt, D. 1998. Localization of glycolipids in membranes by in vivo labeling and neutron diffraction. Mol. Cell 1, 411-419.

Yamamoto, D., Uchihashi, T., Kodera, N., Ando, T. 2008. Anisotropic diffusion of point defects in a two-dimensional crystal of streptavidin observed by high-speed atomic force microscopy. Nanotechnology 19, 1-9.

Figure captions

Fig. 1. AFM images of PM adsorbed onto a mica surface. (A) Low magnification image. PM patches consist of a crystal area (encircled with the dotted line) and a non-crystal area (the periphery of the crystal area). (B) High magnification image of the crystal area showing the packing arrangement of bR molecules at the membrane cytoplasmic surface. The bR trimers (encircled with the triangles) are arranged in a hexagonal lattice with unit cell dimension of ~62 Å. (C) and (D) are successive AFM images of an edge region of PM. Scale bars: (A) 80 nm, (B) 10 nm, and (C, D) 20 nm. Vertical brightness range: (A) 13 nm, (B) 0.8 nm, (C) 7.3 nm, (D) 7.5 nm.

Fig. 2. Time-lapse high-magnification AFM images of the borders between the crystal and non-crystal areas. The bR molecules encircled by the red dotted lines indicate newly bound bR trimer (A), dimer (B) and monomer (C). The white triangles indicate the previously bound trimers

(at 2.1 sec in (A)). Scale bars: (A, B, C) 10 nm. Imaging rate: (A) 3.3 frames/sec, (B, C) 10 frames/sec. Vertical brightness range: (A) 3.8 nm, (B) 2.6 nm, (C) 2.8 nm.

Fig. 3. (A) AFM image of bR crystal with a crevasse. (B) Time-lapse high magnification AFM images on the border between the crystalline and non-ordered areas. The bR trimer highlighted by the red triangle rotated around a pivot (white arrow) formed at the crystal edge (compare the images taken at 0 sec and at 0.24 sec) and then oscillated for ~2 sec. At 2.88 sec, the trimer rotated back to its initial position. (C) Schematic model for the observed AFM images. The positions of W12 in the bR model are indicated by white spheres (PDB 1BRR). The white arrows point at the interaction bonds. The dotted white circle indicates the pivot region for the trimer. Scale bars: (A) 20nm, (B) 10nm. Imaging rate: (A) 2.5 frames/sec, (B) 25 frames /sec. Vertical brightness range: (A) 2.2 nm, (B) 1.4 nm.

Fig. 4. (A) Schematic representation of the binding of a trimer at the crystal edge (I, II, III) and in the crystal interior (VI). Roman numerals indicate the number of interaction bonds (dotted lines) involving the W12 residue. (B, C) Histogram showing the type II and III binding events vs. lifetime. These histograms were fitted with a single-exponential function (red line). The inset in (B) shows the average lifetime as a function of the tip velocity. Error bars indicate the standard deviation for the nonlinear least-square curve fitting.

Appendix A. Supplementary data

Supplementary data associated with this article can be found, in the online version, at…

Supplementary movie captions:

Supplementary movie 1: HS-AFM movie of the crystal edge of a PM captured at an imaging rate of 3.3 frames/sec and scan range of 50×50 nm^2. It is played at double the capture speed. This movie shows the bR trimers binding to and dissociating from the crystal edge.

Supplementary movie 2: HS-AFM movie of pivotal motion captured at an imaging rate of 25 frames/sec and a scan range of 55×34 nm^2. The lower middle bR trimer rotates around a pivot formed at the crystal edge and then oscillates for ~2 sec. The trimer subsequently rotates back to its initial position.

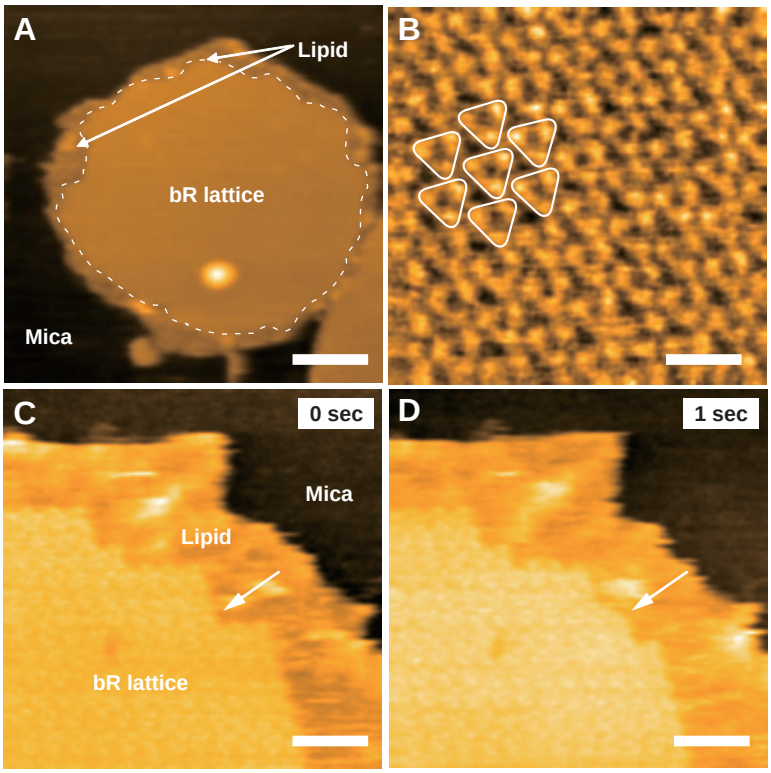
A
Lipid
bR lattice
Mica
B
C
0 sec
Mica
Lipid
bR lattice
D
1 sec

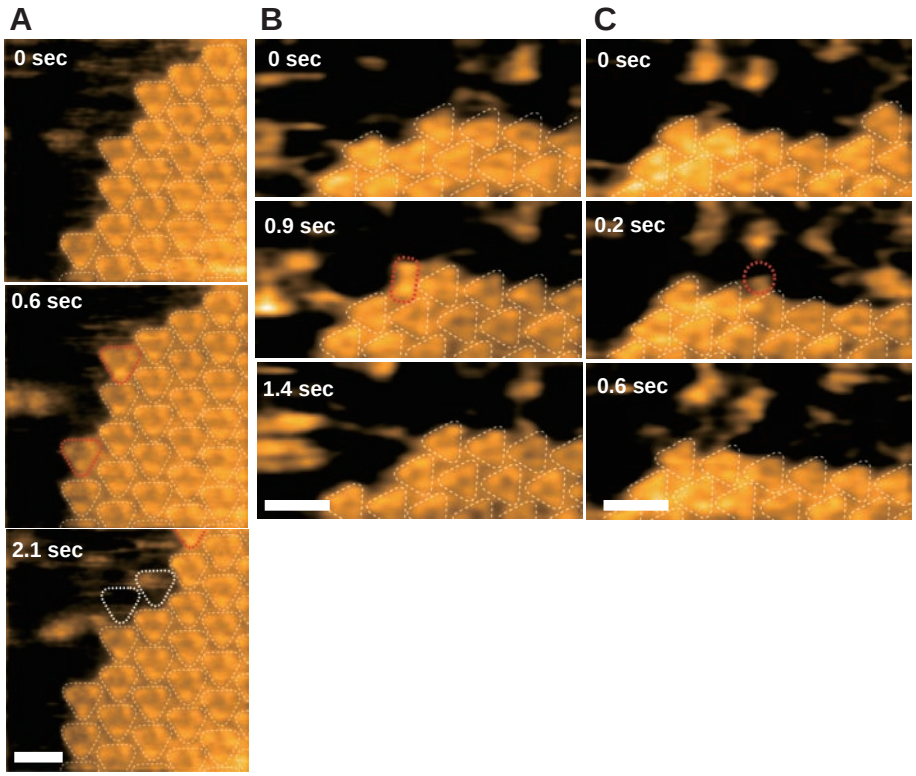
A
B
C
0 sec
0.6 sec
2.1 sec
0 sec
0.9 sec
1.4 sec
0 sec
0.2 sec
0.6 sec

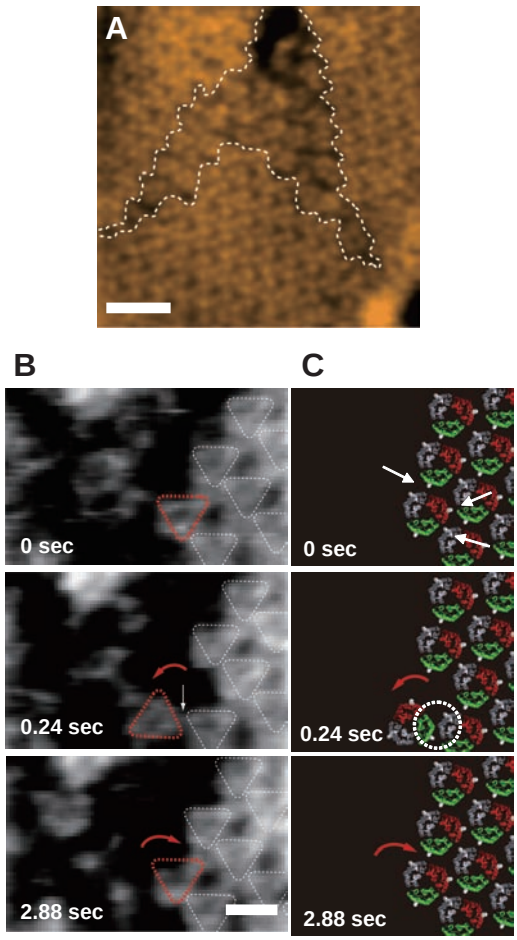
A
B
C
0 sec
0.24 sec
2.88 sec
0 sec
0.24 sec
2.88 sec

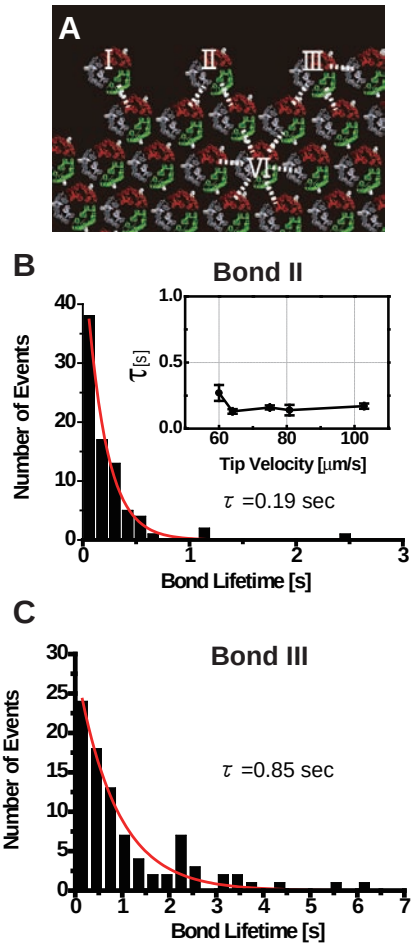
A
I
II
III
VI
B
Bond II
Number of Events
Bond Lifetime [s]
τ =0.19 sec
τ[s]
Tip Velocity [μm/s]
C
Bond III
Number of Events
Bond Lifetime [s]
τ =0.85 sec

Table 1

Observed binding events classified according to the oligomerization states of the newly bound bR.

	Trimer	Dimer	Monomer
Number of events	196	16	27
Fraction (%)	82.0	6.7	11.3